

MAGNETIC RECONNECTION BETWEEN SMALL-SCALE LOOPS OBSERVED WITH THE NEW VACUUM SOLAR TELESCOPE

SHUHONG YANG¹, JUN ZHANG¹, AND YONGYUAN XIANG²

Accepted for publication in ApJL

ABSTRACT

Using the high tempo-spatial resolution H α images observed with the New Vacuum Solar Telescope, we report the solid observational evidence of magnetic reconnection between two sets of small-scale anti-parallel loops with an X-shaped topology. The reconnection process contains two steps: a slow step with the duration of more than several tens of minutes, and a rapid step lasting for only about three minutes. During the slow reconnection, two sets of anti-parallel loops reconnect gradually, and new loops are formed and stacked together. During the rapid reconnection, the anti-parallel loops approach each other quickly, and then the rapid reconnection takes place, resulting in the disappearance of former loops. In the meantime, new loops are formed and separate. The region between the approaching loops is brightened, and the thickness and length of this region are determined to be about 420 km and 1.4 Mm, respectively. During the rapid reconnection process, obvious brightenings at the reconnection site and apparent material ejections outward along reconnected loops are observed. These observed signatures are consistent with predictions by reconnection models. We suggest that the successive slow reconnection changes the conditions around the reconnection site and triggers instabilities, thus leading to the rapid approach of the anti-parallel loops and resulting in the rapid reconnection.

Subject headings: magnetic reconnection — Sun: chromosphere — Sun: evolution

1. INTRODUCTION

Magnetic reconnection is a rearrangement of magnetic field topology, and it is a fundamental physical process in conductive plasma. Magnetic flux is frozen in the plasma except in the small diffusion region where magnetic reconnection takes place (see Zweibel & Yamada 2009; Yamada et al. 2010). When magnetic field lines reconnect, magnetic energy is converted to the thermal energy and kinetic energy of plasmas. According to most of the theories, in the magnetic reconnection, there should exist a small dissipation region, topological changes, strong outflows, and other signatures of magnetic energy release, such as sudden brightenings (e.g., Parker 1957; Sweet 1958; Furth et al. 1963; Petschek 1964). Magnetic reconnection is often considered to be the mechanism driving energy release in solar flares, stellar flares, and many types of jets and outbursts (Rosner et al. 1985; Haisch et al. 1991; Yuan et al. 2009).

The evidences of magnetic reconnection have been observed in different types of solar events, such as flares, coronal mass ejections, and solar wind (Masuda et al. 1994; Gosling et al. 2007; Li & Zhang 2009). Especially, as one of the most energetic phenomena on the Sun, solar flares are widely deemed to be caused by the successive reconnection of magnetic field lines in the corona. Many signatures of magnetic reconnection during flares have been observed, such as cusp-shaped structures above flare loops (Tsuneta et al. 1992), the transformation of “open” loops to closed post-flare ones (Zhang et al. 2013), the reconnection inflows and outflows (Yokoyama

et al. 2001; Innes et al. 2003; Asai et al. 2004; Lin et al. 2005; Takasao et al. 2012; Su et al. 2013). In situ measurements also revealed the occurrence of magnetic reconnection in the magnetosphere (Mozer et al. 2002; Phan et al. 2007; Xiao et al. 2006, 2007; Dunlop et al. 2011). When the magnetic fields carried by solar wind travel outward from the Sun and interact with the planetary magnetic fields, current sheets are created and magnetic reconnection occurs. In laboratories, experiments dedicated to magnetic reconnection have been extensively carried out under controlled conditions (Bratenahl & Yeates 1970; Yamada et al. 1997). With intense lasers in the laboratory, Zhong et al. (2010) reconstructed a magnetic reconnection topology which is similar to that in solar flares. In their experiment, loop-top-like X-ray source emission and outflows were reproduced successfully and the diffusion regions were also identified.

As the primary observing facility of the *Fuxian Solar Observatory* in China, the New Vacuum Solar Telescope (NVST; Liu et al. 2014), a vacuum telescope with a clear aperture of 985 mm, is designed to observe the Sun at high temporal and spatial resolutions. The H α line which is formed in the chromosphere is quite useful to investigate the fine structures of dynamic events. In this Letter, using the NVST H α images, we report a well observed process of magnetic reconnection with two steps between small-scale loops in the chromosphere, which provides observational evidence of magnetic reconnection as predicted in theories.

2. OBSERVATIONS AND DATA ANALYSIS

On 2014 February 3, the NVST was pointed to AR 11967 with a field-of-view (FOV) of $151'' \times 151''$. The NVST data used in this study were obtained in H α 6562.8 Å line from 05:49:52 UT to 09:10:01 UT. The H α images have a cadence of 12 s and a pixel size of $0''.163$. The

¹Key Laboratory of Solar Activity, National Astronomical Observatories, Chinese Academy of Sciences, Beijing 100012, China; shuhongyang@nao.cas.cn

²Fuxian Solar Observatory, Yunnan Observatories, Chinese Academy of Sciences, Kunming 650011, China

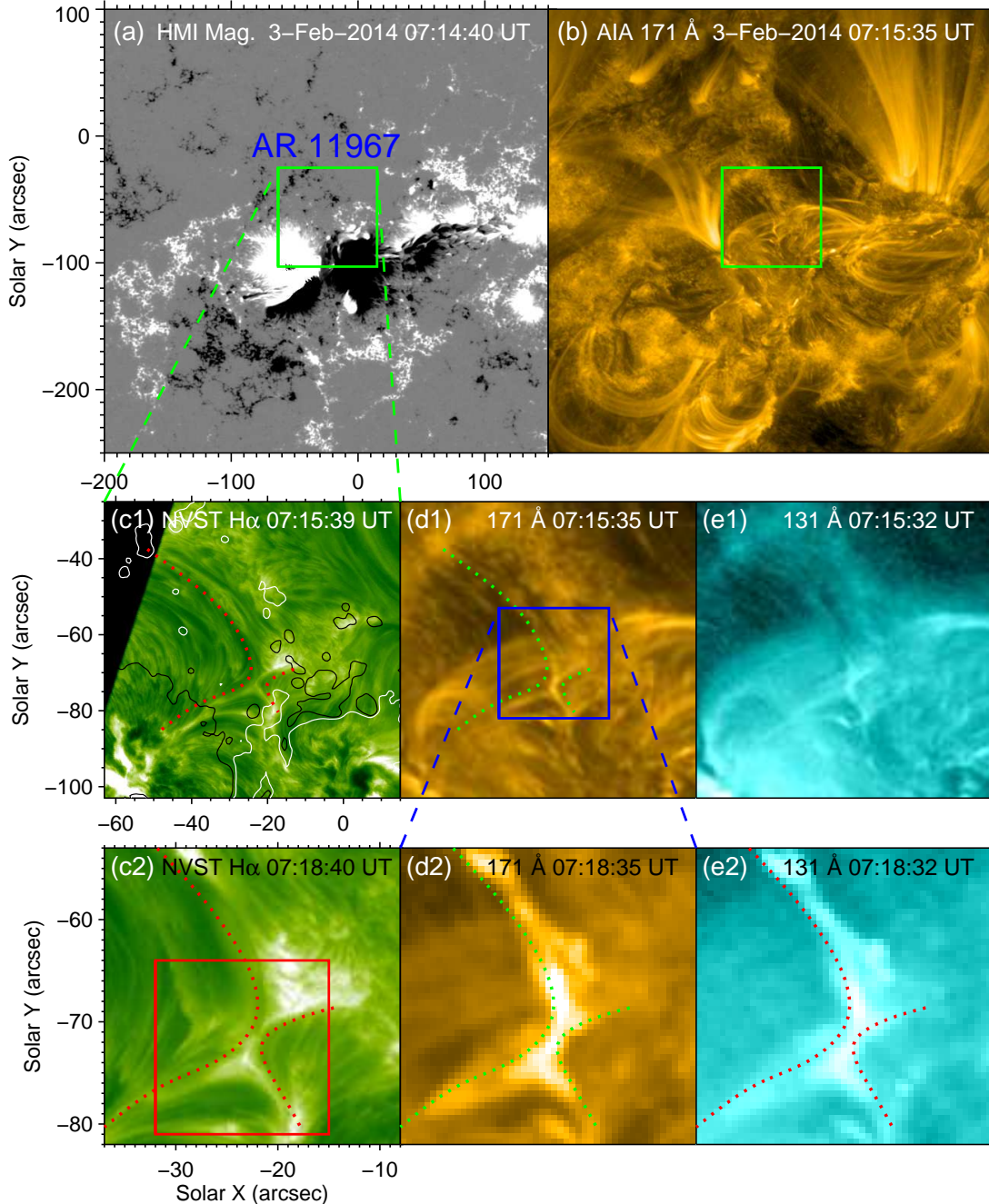


FIG. 1.— Panels (a)-(b): HMI line-of-sight magnetogram and AIA 171 Å image displaying the overview of AR 11967. Panels (c1)-(e1): NVST H α , AIA 171 Å, and 131 Å images showing the expanded view of the area outlined by the square in panel (a). Panels (c2)-(e2): similar to panels (c1)-(e1), but for the area outlined by the square in panel (d1) 3 min later. The red square in panel (c2) outlines the FOV of Figure 2. The black and white curves in panel (c1) are the contours of the positive and negative magnetic fields at levels of 220 G and -220 G, respectively. The red and green dotted curves outline two sets of loops involved in reconnection identified in the H α image.

data are calibrated from Level 0 to Level 1 with dark current subtracted and flat field corrected, and then the calibrated images are reconstructed to Level 1+ by speckle masking (Weigelt 1977; Lohmann et al. 1983). In addition, the Atmospheric Imaging Assembly (AIA; Lemen et al. 2012) multi-wavelength images and the Helioseismic and Magnetic Imager (HMI; Scherrer et al. 2012; Schou et al. 2012) line-of-sight magnetograms from the *Solar Dynamics Observatory* (SDO; Pesnell et al. 2012) are also adopted. We choose the AIA 171 Å and 131 Å

images to study the process of magnetic reconnection at different temperatures. The AIA images were obtained from 05:30 UT to 09:30 UT on February 3 with a pixel size of $0''.6$ and a cadence of 12 s. We use the HMI line-of-sight magnetograms observed from 00:00 UT on February 1 to 00:00 UT on February 5. They have a spatial sampling of $0''.5$ pixel $^{-1}$ and a cadence of 45 s. The AIA and HMI data are calibrated to Level 1.5 by using the standard procedure *aia_prep.pro*, and rotated differentially to a reference time (07:15:00 UT on February 3). Then, we co-align the SDO and NVST images using the cross-correlation method with specific features.

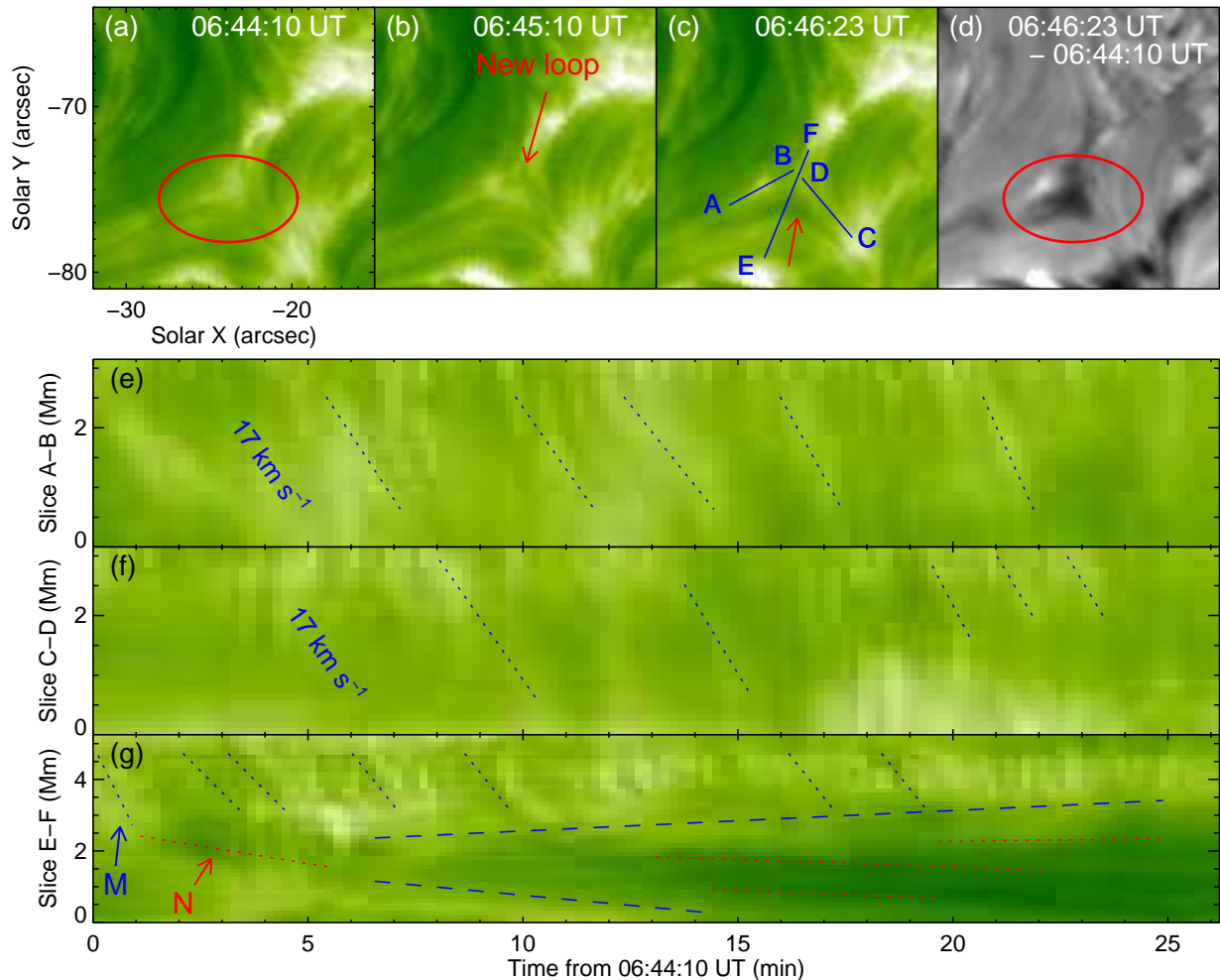


FIG. 2.— Panels (a)-(c): Sequence of H α images showing the formation of a small loop during the slow reconnection process (also see Movie 1). The arrows denote the newly formed loop. Panel (d): difference image between 06:44:10 UT and 06:46:23 UT. The ellipses in panels (a) and (d) outline the area with newly formed H α loop. Panels (e)-(g): space-time plots along slices “A-B”, “C-D”, and “E-F”, respectively, marked in panel (c). The dotted lines in panels (e) and (f) mark the bright moving features, and those in panel (g) follow the dark features. The dashed lines mark the boundaries of the stack of newly formed loops. Arrows “M” and “N” denote the formation and retraction of the H α loop shown in panels (a)-(c).

3. RESULTS

Magnetic reconnection took place at the edge of AR 11967 (see Figure 1(a)). At 07:15 UT, there was a small X-shaped structure at the reconnection site in the AIA 171 \AA image (outlined by the green square in panel (b)), which can be identified more clearly in the expanded view (panel (d1)). In the AIA 131 \AA band this structure was also conspicuous (panel (e1)). The X-shaped structure observed in the EUV images was located between two set of loops (outlined by the dotted curves) identified in the H α image (panel (c1)). It should be mentioned that, as noted by Yang et al. (2014), magnetic loops can be indicated by the dark fibrils in H α images. Here, the reconnection occurred between the loops outlined by the dotted curves. The left loops connected the positive sunspot and the nearby negative fields, and the right loops linked the negative sunspot with the nearby small-scale fields of positive polarity. Three minutes later, the brightness of the X-shaped structure increased significantly in 171 \AA and 131 \AA images (see panels (d2) and (e2)), and there were also some brightenings and changes of H α fibrils (panel (c2)). The reconnection process can be divided

into two steps: a slow step followed by a rapid one.

3.1. Step one: slow reconnection

In the area outlined by the red square in Figure 1(c2), slow reconnection was observed for several tens of minutes, and part of the reconnection is shown in Movie 1. Figures 2(a)-(c) display the formation of a small loop during the slow reconnection process. In our observations, the high-density and low-temperature plasmas may be not sufficiently heated, i.e., some plasmas are heated to high-temperature while others are still at low-temperature. Therefore, newly formed loops can be outlined by either bright or dark features in the outflow regions. In the ellipse region (panel (a)), a being formed loop could be identified at 06:45:10 UT (denoted by the red arrow in panel (b)). At 06:46:23 UT, the newly formed loop was much clearer and reached to a lower site (denoted by the red arrow in panel (c)). In the difference image (panel (d)) between 06:44:10 UT and 06:46:23 UT, there exists a dark structure as outlined by the ellipse, indicating the formation of dark loop.

Along slice “A-B”, “C-D”, and “E-F” marked in panel (c), we make three space-time plots and display them in

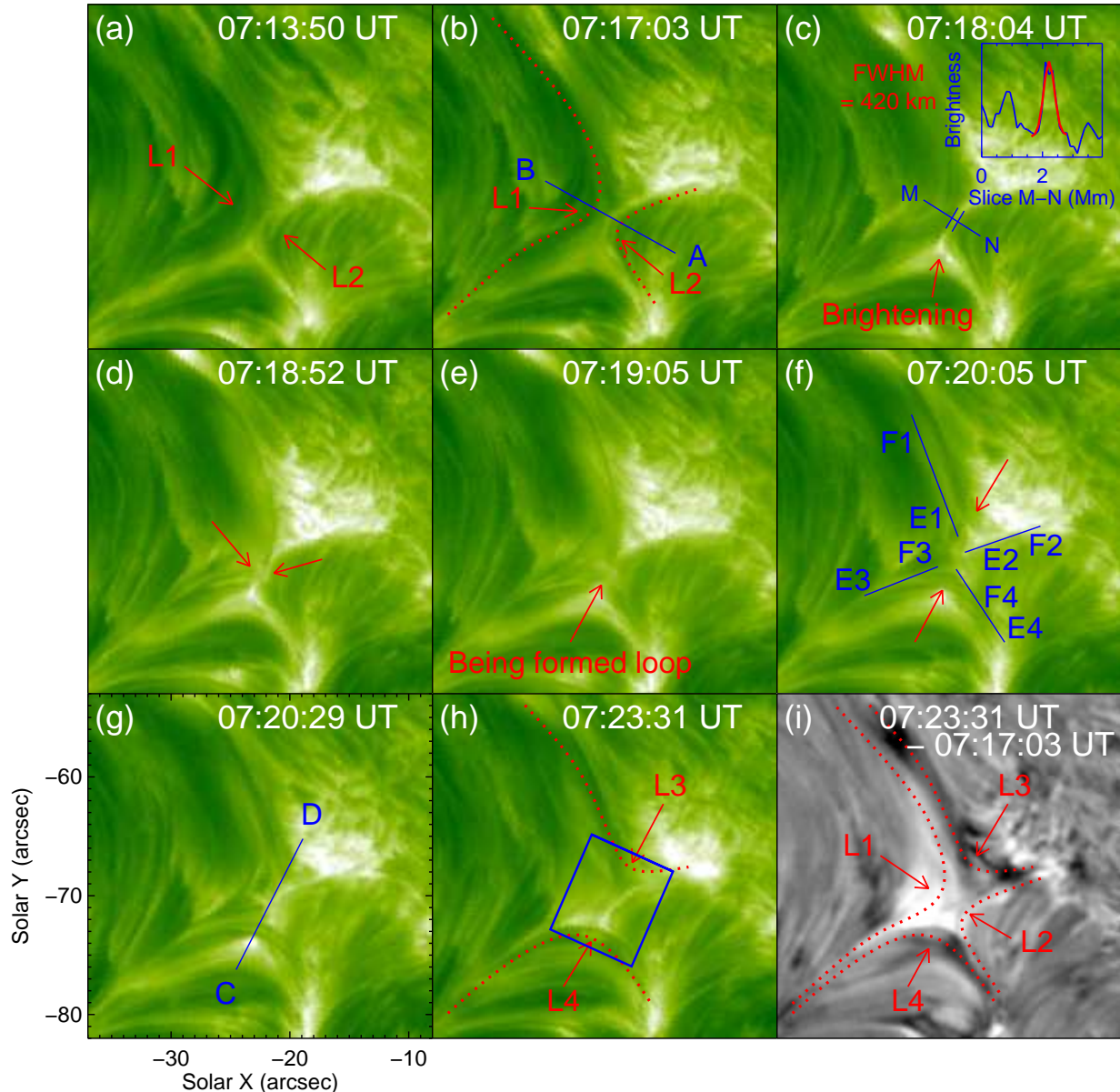


FIG. 3.— Panels (a)-(h): sequence of $H\alpha$ images showing the process of the rapid reconnection (also see Movie 2). Panel (i): difference image between 07:17:03 UT and 07:23:31 UT. Arrows “L1” and “L2” denote the to-be-reconnected loops before reconnection, and arrows “L3” and “L4” denote the newly formed loops after reconnection. The arrow in panel (c) indicates a brightening region, and the two parallel lines mark the reconnection region of interacting loops. The two arrows in panel (d) denote the break points of loops “L1” and “L2”, and the arrows in panels (e) and (f) indicate the being formed loops. The blue square outlines the area where the light curves shown in Figure 4(a) are derived, and the blue lines mark the positions where the space-time plots displayed in Figures 4(b)-(g) are obtained.

panels (e)-(g), respectively. We can see that, there are many bright features, which seem to be the heated blob-like plasmas, moving from “B” to “A”, and from “D” to “C” (as indicated by dotted lines in panels (e) and (f)). The average velocity of the apparent motion of bright features both along “B-A” and “D-C” is about 17 km s^{-1} . In panel (g), the line denoted by arrow “M” indicates the quick downward motion of the newly formed loop shown in panel (b). After the quick motion, the new loop continued to move downward slowly, as denoted by arrow “N”. As the reconnection went on, more and more new loops were formed and stacked together (see the other blue and red dotted lines in panel (g)). The boundaries of the loop stack are marked by the dashed lines.

3.2. Step two: rapid reconnection

Figure 3 shows the process of the rapid reconnection (also see Movie 2). The loops involved into the reconnection are labeled with “L1” and “L2”, as denoted by the arrows in panels (a) and (b). Before the occurrence of the rapid reconnection, the two sets of loops were approaching each other. At 07:17:03 UT, the distance between loops “L1” and “L2” was much shorter than that at 07:13:50 UT. Then loops “L1” and “L2” continued to move to each other and eventually interacted. At 07:18:04 UT, an obvious brightening (denoted by the arrow in panel (c)) can be observed. The two short parallel lines mark the reconnection region of the interacting loops. The inserted blue curve shows the brightness along slice “M-N”, and the overlaid red curve is the Gaus-

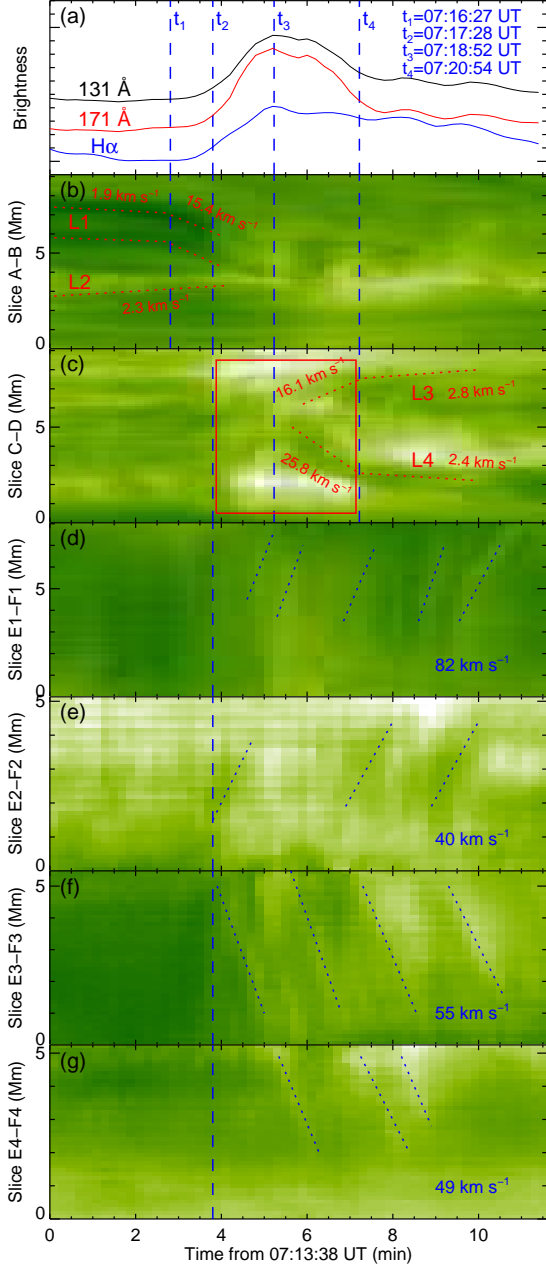


FIG. 4.— Panel (a): light curves in H α , 171 Å, and 131 Å lines derived from the area outlined by the square in Figure 3(h). Panels (b)-(g): space-time plots along slices “A-B”, “C-D”, “E1-F1”, “E2-F2”, “E3-F3”, and “E4-F4”, respectively, marked in Figure 3. The dotted lines “L1” and “L2” display the evolution of the loops before reconnection, and “L3” and “L4” denote that of the new loops. The blue dotted lines in panels (d), (f), and (g) follow the bright features, and those in panel (e) follow the dark features. The vertical dashed lines label the different stages of the rapid reconnection. The rectangle in panel (c) outlines the brightenings during the reconnection process.

sian fit of the brightness profile. The width of the bright interaction region is given by the width of the Gaussian, which is found to be 420 km. The length (presented by the length of the parallel lines) of the interaction region is about 1.4 Mm. At 07:18:52 UT, both loops “L1” and “L2” broke apparently (as denoted by the two arrows in panel (d)). Only 13 s later, a new loop had been formed, as denoted by the arrow in panel (e). At 07:20:05 UT, the new loop was more conspicuous (indicated by the lower

arrow in panel (f)) and another new loop (denoted by the higher arrow) can also be observed. Then the two new loops retracted and moved away from each other (panels (g)-(h)). The difference image between 07:17:03 UT and 07:23:31 UT is displayed in panel (i). In the difference image, the locations of the former loops “L1” and “L2” are white structures, which is caused by the disappearance of loops “L1” and “L2”. While the black structures are coincided with the locations of loops “L3” and “L4”, indicating the formation of new H α loops.

During the rapid reconnection process, the most remarkable changes are the disappearance of loops “L1” and “L2” and the formation of loops “L3” and “L4”. To clearly display these changes with time, we make two space-time plots along slices “A-B” and “C-D” which are marked in Figure 3, and display them in Figures 4(b) and (c). When the reconnection began, we can find apparent ejections of bright features outward along “E1-F1”, “F3-E3” and “F4-E4”, and dark features along “E2-F2” (marked in Figure 3) from the reconnection site. It should be noted that, as displayed in Figure 3(f), the background of slice “E2-F2” is so bright that the expected bright moving features could not be distinguished, while some dark features can be identified. Then we derive four space-time plots along the four slices and exhibit them in Figures (d)-(g), respectively. We also measure the brightness variations of H α , 171 Å, and 131 Å images in the region outlined by the rectangle in Figure 3(h), and the corresponding light-curves are shown in Figure 4(a). Before 07:16:27 UT (t_1 , indicated by the leftmost vertical line in Figure 4), loop “L1” approached loop “2” slowly with an average velocity of 1.9 km s⁻¹ (see panel (b)). While after t_1 , loop “L1” moved toward loop “L2” quickly with a velocity of 15.4 km s⁻¹, and contacted each other at 07:17:28 UT (t_2 , the second vertical line). Before t_2 , there was no obvious variation for the brightness in each wavelength (panel (a)), and no significant moving feature along different directions (panels (d)-(g)). After t_2 , when loop “L1” began to interact with loop “L2” (panel (b)), the brightness in each wavelength increased rapidly (see panel (a)). At and around the reconnection region, the brightenings in H α , 171 Å, and 131 Å lines can be found in panels (a) and (c) and Movie 2. All the three light curves reach the maximum at the same time, i.e., 07:18:52 UT (t_3 in panel (a)). Also at that time, loops “L1” and “L2” disappeared (see panel (b)) and loops “L3” and “L4” began to be formed (panel (c)). From t_3 , the light curves exhibit a decrease trend (panel (a)), and the newly formed loops separated quickly with a separation velocity of 42 km s⁻¹ (panel (c)). When the reconnection ended at around 07:20:54 UT (t_4), the brightenings in multi-wavelengths almost disappeared (see panels (a) and (c) and Movie 2). The separation velocity also slowed down to about 5.2 km s⁻¹ (as indicated by the dotted curves in panel (c)). In panels (d)-(g), moving features only can be identified after t_2 , i.e., the start time of the rapid reconnection. The apparent motions of small features along all of the four directions can be observed, and they have a comparable velocity of about 50 km s⁻¹.

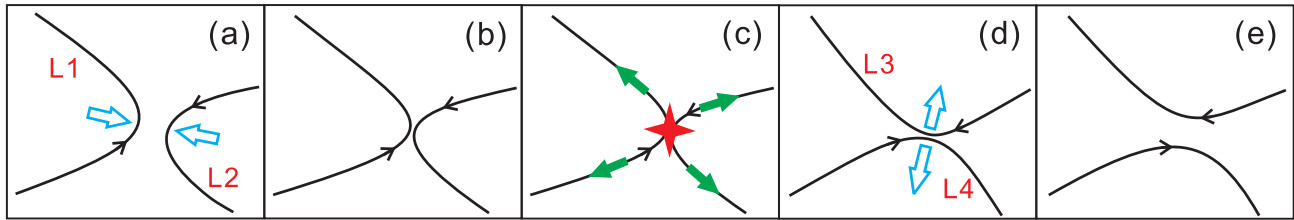


FIG. 5.— Schematic drawings illustrating the magnetic reconnection process observed in this study. The blue arrows in panel (a) indicate the convergence of loops “L1” and “L2”, and the blue arrows in panel (d) indicate the separation of the newly formed loops “L3” and “L4”. In panel (c), the red symbol marks the reconnection site, and the green arrows represent the material ejections due to the reconnection.

Using the NVST $H\alpha$ images with high tempo-spatial resolutions, we have observed signatures of magnetic reconnection between two sets of small-scale loops. The reconnection process can be divided into two steps: a slow reconnection with the duration of several tens of minutes and a rapid reconnection lasting for only about three minutes. During the slow reconnection process, two sets of anti-parallel loops gradually reconnected, and new loops were formed and stacked together. During the rapid reconnection, the anti-parallel loops moved toward each other quickly, and then the rapid reconnection took place, resulting in the disappearance of former loops. In the meantime, new loops were formed and separated. During the rapid reconnection process, we have observed obvious brightenings at the reconnection site and apparent ejections of bright or dark features outward along the newly formed loops with an average velocity of about 50 km s^{-1} .

According to the observational results, we sketch a series of cartoons (see Figure 5) to illustrate the reconnection process. The loops “L1” and “L2” which will be reconnected move toward each other to a very close distance, as shown in panels (a) and (b). When the loops are close enough (about 420 km determined in this study), magnetic reconnection between them takes place. At the reconnection site, brightenings are observed, and along different directions, apparent ejections of small features outward from the reconnection site can be observed (see panel (c)). Then two new loops “L3” and “L4” are formed while the former loops “L1” and “L2” have disappeared, and the newly formed loops begin to separate (panels (d) and (e)). The common features of most reconnection theories include the changes of magnetic topologies and the release of magnetic energy (Parker 1957; Sweet 1958; Petschek 1964; see the review by Yamada et al. 2010). The topology changes are mainly the break of inflowing anti-parallel loops and the formation of new loops. When the loops reconnect in the diffusion region, magnetic energy is released, thus heating the plasmas. The plasma pressure is raised, and a great deal of energy is converted to the kinetic energy. In addition, the reconnected field lines near the X-point are sharply bent and the magnetic tension force also impacts on the plasmas to increase the kinetic energy. Therefore, the plasmas are brightened and expelled. All the above features which should appear in the magnetic reconnection have been observed in the present study. Our results are highly consistent with the common models of magnetic reconnection.

Until now, many evidences of magnetic reconnection on

the Sun have been reported by many authors (Tsuneta et al. 1992; Yokoyama & Shibata 1995; Yang et al. 2011; Takasao et al. 2012; Cirtain et al. 2013). However, most of these observational signatures of magnetic reconnection have been found in solar eruptive events. According to the popular flare model, a rising flux rope in the corona stretches the overlying magnetic fields lines, and a current is created between the anti-parallel field lines and magnetic reconnection occurs (Shibata et al. 1995; Tsuneta 1996; Lin & Forbes 2000). In the present study, the magnetic reconnection is observed in a relative stable X-shaped structure in the chromosphere compared with that observed during flares in the corona. The previous observations have revealed that the current sheets have a thickness $> 10^4 \text{ km}$ and a length of more than several hundreds of Mm (Ciaravella & Raymond 2008; Lin et al. 2009). In the present study, the thickness and length of the brightening region between the approaching loops are only about 420 km and 1.4 Mm, respectively. It is likely that a current sheet is embedded inside this structure of enhanced emission. If so, the current sheet determined in this study is much smaller than those previously reported.

In our observations, the reconnection process includes two steps, i.e., a slow reconnection followed by a rapid reconnection. The slow reconnection lasted for several tens of minutes, while the rapid step only took about three minutes. We suggest that the continual slow reconnection changed the conditions around the reconnection region which triggered instabilities and led to rapid approaching of the anti-parallel loops, thus resulting in the rapid reconnection. A similar scenario was also proposed in the flare events by Wang & Shi (1993). They suggested that there is a slow reconnection between two topologically separated loops in the lower atmosphere and the slow reconnection triggers the fast reconnection in the corona which is responsible for large solar activities.

This work is supported by the National Natural Science Foundations of China (11203037, 11221063, 11303049, and 11373004), the Outstanding Young Scientist Project 11025315, the CAS Project KJCX2-EW-T07, the National Basic Research Program of China under grant 2011CB811403, and the Strategic Priority Research Program—The Emergence of Cosmological Structures of the Chinese Academy of Sciences (No. XDB09000000). The data are used by courtesy of NVST, AIA, and HMI science teams.

REFERENCES

- Ciaravella, A., & Raymond, J. C. 2008, *ApJ*, 686, 1372
- Cirtain, J. W., Golub, L., Winebarger, A. R., et al. 2013, *Nature*, 493, 501
- Dunlop, M. W., Zhang, Q.-H., Bogdanova, Y. V., et al. 2011, *Physical Review Letters*, 107, 025004
- Furth, H. P., Killeen, J., & Rosenbluth, M. N. 1963, *Physics of Fluids*, 6, 459
- Gosling, J. T., Phan, T. D., Lin, R. P., & Szabo, A. 2007, *Geophys. Res. Lett.*, 34, 15110
- Haisch, B., Strong, K. T., & Rodono, M. 1991, *ARA&A*, 29, 275
- Innes, D. E., McKenzie, D. E., & Wang, T. 2003, *Sol. Phys.*, 217, 267
- Lemen, J. R., Title, A. M., Akin, D. J., et al. 2012, *Sol. Phys.*, 275, 17
- Li, L. P., & Zhang, J. 2009, *ApJ*, 703, 877
- Lin, J., & Forbes, T. G. 2000, *J. Geophys. Res.*, 105, 2375
- Lin, J., Li, J., Ko, Y.-K., & Raymond, J. C. 2009, *ApJ*, 693, 1666
- Lin, J., Ko, Y.-K., Sui, L., et al. 2005, *ApJ*, 622, 1251
- Liu, Z., Xu, J., Gu, B.-Z., et al. 2014, *Research in Astronomy and Astrophysics*, 14, 705
- Lohmann, A. W., Weigelt, G., & Wirtitzer, B. 1983, *Appl. Opt.*, 22, 4028
- Masuda, S., Kosugi, T., Hara, H., Tsuneta, S., & Ogawara, Y. 1994, *Nature*, 371, 495
- Mozer, F. S., Bale, S. D., & Phan, T. D. 2002, *Physical Review Letters*, 89, 015002
- Parker, E. N. 1957, *J. Geophys. Res.*, 62, 509
- Pesnell, W. D., Thompson, B. J., & Chamberlin, P. C. 2012, *Sol. Phys.*, 275, 3
- Petschek, H. E. 1964, *NASA Special Publication*, 50, 425
- Phan, T. D., Paschmann, G., Twitty, C., et al. 2007, *Geophys. Res. Lett.*, 34, 14104
- Rosner, R., Golub, L., & Vaiana, G. S. 1985, *ARA&A*, 23, 413
- Scherrer, P. H., Schou, J., Bush, R. I., et al. 2012, *Sol. Phys.*, 275, 207
- Schou, J., Scherrer, P. H., Bush, R. I., et al. 2012, *Sol. Phys.*, 275, 229
- Shibata, K., Masuda, S., Shimojo, M., et al. 1995, *ApJ*, 451, L83
- Su, Y., Veronig, A. M., Holman, G. D., et al. 2013, *Nature Physics*, 9, 489
- Sweet, P. A. 1958, *Electromagnetic Phenomena in Cosmical Physics*, 6, 123
- Takasao, S., Asai, A., Isobe, H., & Shibata, K. 2012, *ApJ*, 745, L6
- Tsuneta, S. 1996, *ApJ*, 456, 840
- Tsuneta, S., Hara, H., Shimizu, T., et al. 1992, *PASJ*, 44, L63
- Wang, J. X., & Shi, Z. X. 1993, *Sol. Phys.*, 143, 119
- Weigelt, G. P. 1977, *Optics Communications*, 21, 55
- Xiao, C. J., Wang, X. G., Pu, Z. Y., et al. 2006, *Nature Physics*, 2, 478
- Xiao, C. J., Wang, X. G., Pu, Z. Y., et al. 2007, *Nature Physics*, 3, 609
- Yamada, M., Ji, H., Hsu, S., et al. 1997, *Physics of Plasmas*, 4, 1936
- Yamada, M., Kulsrud, R., & Ji, H. 2010, *Reviews of Modern Physics*, 82, 603
- Yang, S. H., Zhang, J., Li, T., & Liu, Y. 2011, *ApJ*, 732, L7
- Yang, S. H., Zhang, J., & Xiang, Y. Y. 2014, *ApJ*, 793, L28
- Yuan, F., Lin, J., Wu, K., & Ho, L. C. 2009, *MNRAS*, 395, 2183
- Yokoyama, T., Akita, K., Morimoto, T., Inoue, K., & Newmark, J. 2001, *ApJ*, 546, L69
- Yokoyama, T., & Shibata, K. 1995, *Nature*, 375, 42
- Zhang, J., Yang, S. H., Li, T., et al. 2013, *ApJ*, 776, 57
- Zhong, J. Y., Li, Y., Wang, X., et al. 2010, *Nature Physics*, 6, 984
- Zweibel, E. G., & Yamada, M. 2009, *ARA&A*, 47, 291